View metadata, citation and similar papers at core.ac.uk

brought to you by CORE

provided by Apollo

Nanoscale

PAPER

Impact of oxygen exchange reaction at the ohmic interface in Ta_2O_5-based ReRAM devices

Received 00th January 20xx,
Accepted 00th January 20xx

DOI: 10.1039/x0xx00000x

www.rsc.org/

Wonjoo Kim [a], Stephan Menzel [a], Dirk J. Wouters [b], Bernd Roesgen [a], John Robertson [c], Rainer Waser [a, b] and Vikas Rana [a]

Interface reactions constitute essential aspects of the switching mechanism in redox-based resistive random access memory (ReRAM). For example, the modulation of the electronic barrier height at the Schottky interface is considered to be responsible for the toggling of the resistance states. On the other hand, the role of the ohmic interface in the resistive switching behavior is still ambigious. In this paper, the impact of different ohmic metal-electrode (M) materials, namely W, Ta, Ti, and Hf on the characteristics of Ta_2O_5 ReRAM is investigated. These materials are chosen with respect to their free energy for metal oxide formation and, associated, their impact on the formation energy of oxygen vacancy defects at the M/Ta_2O_5 interface. The resistive switching devices with Ti and Hf electrodes that have a negative defect formation energy, show an early RESET failure during the switching cycles. This failure process with Ti and Hf electrode is attributed to the accumulation of oxygen vacancies in the Ta_2O_5 layer, which leads to permanent breakdown of the metal-oxide to a low resistive state. In contrast, the defect formation energy in the Ta_2O_5 with respect to Ta and W electrodes is positve and for those highly stable resistive switching behavior is observed. During the quasi-static and transient-pulse characterization, the ReRAM devices with the W electrode consistently show a increased high resistance state (HRS) than with the Ta electrode for all RESET stop voltages. This effect is attributed to the faster oxygen exchange reaction at the W-electrode interface during the RESET process in accordance to lower stability of WO_3 than Ta_2O_5. Based on these findings, an advanced resistive switching model, wherein also the oxygen exchange reaction at the ohmic M-electrode interface plays a vital role in determining of the resistance states, is presented.

Introduction

Redox-based resistive random access memory (ReRAM) is considered as a strong candidate to compete against conventional non-volatile memories such as NAND flash memory for mass storage application because of its lower power consumption, fast switching speed and down-scaling under 20 nm [1-3]. Metal-oxide based bipolar ReRAM devices consist of an insulating switching layer stacked between two asymmetric metal electrodes: one low work function (WF) ohmic electrode (OE) (which is also easily oxidizable), such as W, Ti, Hf, or Ta, and a high WF (inert) metal electrode, such as Pt. The resistive switching mechanism relies on the motion of mobile ionic defects under the applied electrical field. While motion of metal cations has been evidenced and their role cannot be excluded [4], the most widely accepted model is based on (double) positively charged oxygen vacancy defects Vö. These V_O's are introduced in the switching layer during the initial forming step, which results in the formation of a filamentary region with a high concentration of oxygen vacancies between these two electrodes. The main process of V_O defect generation during forming is thought to be extrinsic defect generation due to oxygen excorporation (Equation 1, following the Kröger-Vink notation [5]):

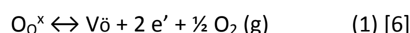

$$O_O^x \leftrightarrow V\ddot{o} + 2\,e' + ½\,O_2\,(g) \qquad (1)\ [6]$$

When the electrons are localized at the metal cations, (1) becomes:

$$O_O^x + 2\,M_M^x \leftrightarrow V\ddot{o} + 2\,M_M' + ½\,O_2\,(g) \qquad (2)$$

The presence of the Vö, by a local redox reaction, changes the valence of the neighbouring metal cations in the metal oxide film (Note that the Kröger-Vink notation only lists relative charges, with the metal here changing from neutral to negative. In absolute charge notation, the cation may go e.g. from charge state 5+ to 4+), hence, it is termed as valence change memory or VCM.

Besides the forming process (Eq. 1), the V_O's are also introduced during processing by oxygen exchange between the oxide layer and the OE layer, i.e. oxygen is extracted from the metal oxide (MO) and

a. Peter Grünberg Institute, Forschungszentrum Jülich GmbH, 52425 Jülich, Germany and also with JARA—Fundamentals in Future Information Technology (E-mail: w.kim@fz-juelich.de).
b. Institute of Materials in Electrical Engineering and Information Technology II, RWTH Aachen University, 52074 Aachen, Germany.
c. Electronic Devices & Materials (EDM) Group, Department of Electrical Engineering, University of Cambridge, United Kingdom

†Electronic Supplementary Information (ESI) available: [details of any supplementary information available should be included here]. See DOI: 10.1039/x0xx00000x

Please do not adjust margins

oxidizes the OE metal (=M*) to the formation of M*-oxide, see Equation 3 (for notation, $M_{M(MO)}$ stands for an M atom on a M-metal site in the MO metal-oxide, while $M^*_{M^*(M^*)}$ stands for an M* atom on a M*-metal site in the M* metal etc.). Here, it is assumed that the M* oxidizes to valence +4, i.e. forms a new phase M^*O_2:

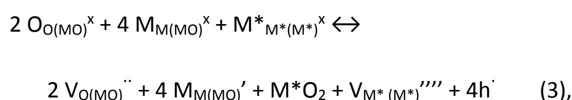

$$2\,O_{O(MO)}^{x} + 4\,M_{M(MO)}^{x} + M^*_{M^*(M^*)}{}^{x} \leftrightarrow 2\,V_{O(MO)}^{\cdot\cdot} + 4\,M_{M(MO)}' + M^*O_2 + V_{M^*(M^*)}'''' + 4h^{\cdot} \quad (3),$$

In case, the cap layer is already partly oxidized at the interface (to $M^*O_{2-\delta}$), as e.g. during device operation, the oxygen exchange corresponds to a reverse V_O exchange, see equation (4):

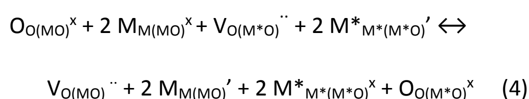

$$O_{O(MO)}^{x} + 2\,M_{M(MO)}^{x} + V_{O(M^*O)}^{\cdot\cdot} + 2\,M^*_{M^*(M^*O)}{}' \leftrightarrow V_{O(MO)}^{\cdot\cdot} + 2\,M_{M(MO)}' + 2\,M^*_{M^*(M^*O)}{}^{x} + O_{O(M^*O)}^{x} \quad (4)$$

The oxygen exchange with the OE during deposition introduces a high concentration of the V_O located in the oxide film near the OE electrode (so called defect "reservoir"). The resultant introduction of V_O in the oxide film lowers the initial resistance and the forming voltage of the device. For a Pt/$SrTiO_3$/Ti VCM cell, it is demonstrated that the forming voltage depends on $SrTiO_3$/Ti layer thickness ratio [7]. The $SrTiO_3$ layer is further chemically reduced by a thicker Ti layer, which finally leads to an electroforming-free device. Most switching models, however, presume that during the RESET/SET switching process, only a redistribution of the V_O within the oxide layer takes place keeping the total amount of the V_O's constant, i.e. no further oxygen exchange with the OE takes place during the switching process.

As mobile donors, the Vö's can influence the overall resistance of the ReRAM cell in two ways. First, the local conductivity of the metal-oxide film increases with increasing V_O concentration [V_O] [8-10]. Second, the electrostatic barrier heights at the high WF metal/oxide interface are modulated by the local V_O concentration due to the Schottky effect [11-13]. During the RESET/SET switching (applying positive/negative bias to the inert electrode), the V_O's move away/towards the interface with the high WF electrode (in accordance with disrupting/restoring the filament). It is assumed that the OE forms an Ohmic contact with the metal-oxide layer, whereas in absence of a high concentration of Vö (disrupted filament) the high WF metal forms high Schottky barrier that dominates the overall resistance in the high resistive state (HRS). During the SET operation, the V_O's move to the high WF, where the increased V_O concentration lowers the Schottky barrier and the device switches to the low resistive state (LRS). Hence, interfacial conduction strongly affects the resistive values in the different states of the oxide ReRAM [14, 15].

In this study, we analyzed Ta_2O_5-based ReRAM devices using different OE materials (W, Ta, Ti and Hf). Among various oxide switching materials, the Ta_2O_5-based ReRAMs exhibit excellent performance in switching speed [16], endurance[1, 17], retention [18] and low power [19-21]. The OE materials are chosen for the defect formation energy of oxygen vacancy (E_{VO}) with respect to the Ta_2O_5 layer. For the Hf and the Ti, this E_{VO} is negative, whereas it is positive for the Ta and the W. In this experiment, we have observed that the OE not only affects the forming voltage but also the RESET process. The devices with the Hf and the Ti electrode show an early RESET failure, whereas the devices with the Ta and the W OE show highly reliable switching behaviour. The Pt/Ta_2O_5/W ReRAM devices show faster RESET process than the Pt/Ta_2O_5/Ta, which leads to higher R_{HRS}/R_{LRS} ratio under the same bias conditions. These observations indicate that oxygen interchange with the OE plays an important role during the resistive switching process. Based on these findings, an advanced resistive switching model, where the oxygen exchange reaction at the OE interface plays a vital role in determining of the resistance states, is presented.

Experimental

In this study, 5 nm-thick Titanium (Ti) and 30 nm-thick Platinum (Pt) layers are deposited by sputtering on a thermally grown 450 nm-thick SiO_2 layer on Si substrate. Next, photolithography and dry-etching processes are used to pattern the Pt layer as bottom electrode. After the patterning, 7 nm-thick Ta_2O_5 is deposited by reactive sputtering under a process gas mixture of argon (77%) and oxygen (23%) with an RF power of 116 W at a chamber pressure of 2.3×10^{-2} mbar. Without breaking the vacuum, a 13 nm-thick OE and a 25 nm-thick Pt layer are deposited by RF and DC sputtering, respectively. In this experiment, four different OE layers, i.e. W, Ta, Ti and Hf are used. All deposition processes are performed at room temperature. To pattern the top electrode, photolithography with positive photo-resist is applied. After the photo-resist

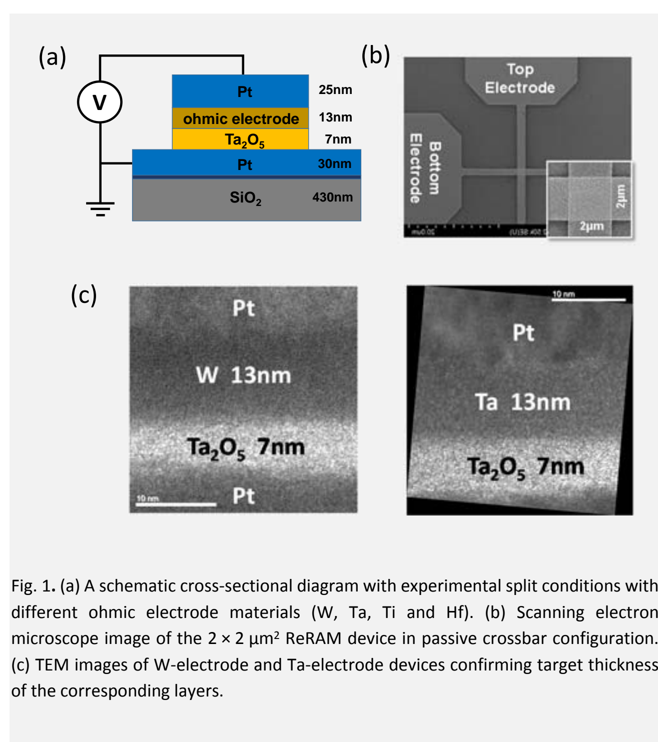

Fig. 1. (a) A schematic cross-sectional diagram with experimental split conditions with different ohmic electrode materials (W, Ta, Ti and Hf). (b) Scanning electron microscope image of the 2 × 2 µm² ReRAM device in passive crossbar configuration. (c) TEM images of W-electrode and Ta-electrode devices confirming target thickness of the corresponding layers.

This journal is © The Royal Society of Chemistry 20xx

Please do not adjust margins

Please do not adjust margins

development, the top electrode is etched down with Reactive Ion Beam Etching (RIBE). This step leads to the Pt/Ta_2O_5/OE/Pt ReRAM device sketched in Fig. 1(a). A SEM image of the patterned passive crossbar structure with 2 × 2 μm^2 device junction is shown in Fig. 1(b). The cross-sectional TEM images of the ReRAM devices with the Ta-OE and the W-OE layer confirm the thicknesses of corresponding device stacks in Fig. 1(c). The device characterization is performed using the Keithley 4200SCS under atmospheric conditions at room temperature.

V_O defect formation energies of used stacks

The driving force of the interfacial chemical reaction (see eq. 3) is related to the energy of oxygen vacancy defect formation (E_{VO}) in the metal oxide at the OE interface [22-24]. Recently, Guo *et al.* calculated E_{VO} in different metal oxides, and for different metal cap layers [25, 26]. In these defect energy calculations, they made a difference between O-rich and O-poor conditions. The O-rich conditions actually apply to the metal oxide exposed to oxygen ambient (with atmospheric pO_2). The O-poor condition corresponds to the metal-oxide in contact with an OE layer of the same metal as the oxide host metal (M*=M). In that case, the energy required for removing the O from the metal oxide is nearly completely compensated by the (negative) free energy of oxidation of the metal cap, and the resultant defect formation energy is approximately 0. Fig. 2(a) shows the calculated E_{VO} values in HfO_2 and Ta_2O_5 in contact with different OE (based on Fig. 5 of [27], where the energy values for the Hf and the Ti with respect to the Ta_2O_5 have been extrapolated based on available data in the reference [25, 26]. Based on these calculations, the E_{VO} for the Ta_2O_5 layer is estimated to be 1.4 eV for W-electrode, 0.1 eV for Ta-electrode. -0.6 eV for Ti-electrode and -1.5 eV for Hf-electrode. In general, as depicted in Fig. 2(a), the E_{VO} increases with the stability (i.e. lower free energy of oxide formation) of the host oxide (cf. parallel shift of defect energy for Ta_2O_5 and HfO_2), and decreases according to the stability of the metal cap oxide (horizontal shift according to OE metal used. The O chemical potential corresponds to the equilibrium oxygen partial pressure of the M*/M*O couple, reflecting the relative M*O stability). It can be observed that a cap metal that has a more stable oxide than the oxide host metal (e.g., Ta_2O_5 capped with Hf and Ti) results in a negative E_{VO}. A positive E_{VO} is required for stable switching [27], as the negative E_{VO} would result in a continuous increase of the V_O in the switching film, resulting in a non-switchable, conducting film.

Forming and switching properties

The influence of the OE on the forming voltage was investigated by measuring 50 devices for each device stack. The forming process was performed by a positive DC voltage sweep (+3 V) applied to the OE with a current compliance (I_{CC}) of 1.0 mA. The forming statistics of the four different device stacks are given in Fig. 2(b). A clear dependence of the forming voltage on the ohmic electrode material is observed. The lowest forming voltage is observed for the Hf-electrode devices (V_{Form} = 0.84 V in median), followed by the Ti-

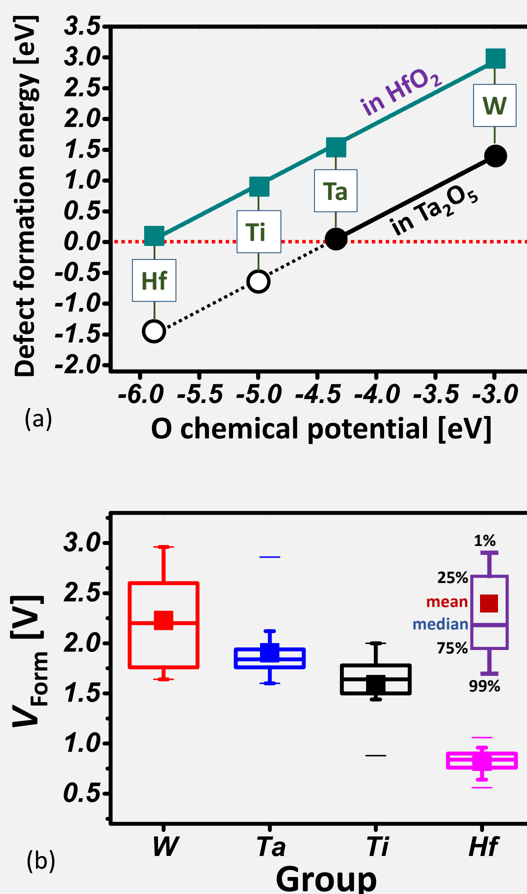

Fig. 2. (a) Interfacial defect formation energy for oxygen vacancy defects E_{VO} in Ta_2O_5 and HfO_2 as function of the oxygen chemical potential. This chemical potential is determined by the ohmic electrode present as indicated here for Ta, W, Ti and Hf. (b) Forming voltage of the Ta_2O_5 ReRAM device for each ohmic metal electrode (W, Ta, Ti and Hf)

electrode devices (V_{Form} = 1.64 V in median). The W-electrode devices show the highest forming voltage (V_{Form} = 2.21 V in median) followed by the Ta-electrode ones (V_{Form} = 1.84 V in median). These forming voltage trends as shown in Fig. 2(b) clearly correspond with the oxygen vacancy defect formation energies at the respective OE/Ta_2O_5 interfaces as shown in Fig. 2(a). During the switching, the ReRAM devices with the Ti- and the Hf-OE show a failure in the RESET process within the first 20 cycles. This early RESET failure is shown in Fig. 3(a). The gray lines show the switching behavior of the Ta_2O_5 ReRAM with the Ti- and the Hf-OE before failure. After the RESET failure the ReRAM devices exhibit ohmic *I-V* behavior and are stuck in the LRS regime. In contrast, stable switching operation has been observed with the W- and the Ta-OE under the same biasing conditions as shown in Fig. 3(b). Average switching curves are shown in red for the W-OE and in blue for the Ta-OE devices. The occurrence of RESET failure or stable switching clearly correlates with (the sign of) E_{VO} at the OE/Ta_2O_5 interface, suggesting that oxygen exchange takes place at this OE/Ta_2O_5 interfaces during switching. This will be discussed with more details in the latter part of this study.

Please do not adjust margins

Please do not adjust margins

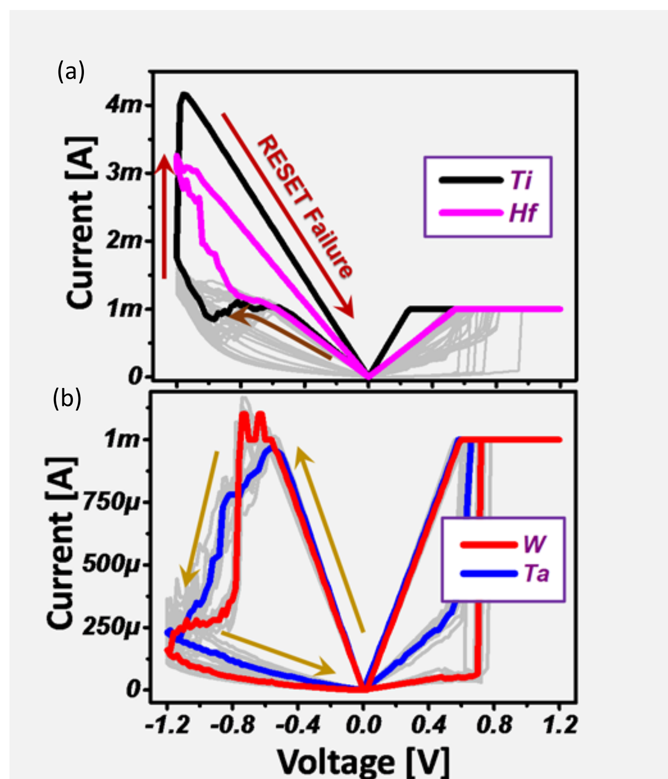

Fig. 3. At the given I_{CC} of 1.0 mA, the switching curves of Ta_2O_5 ReRAM with different OE and the maximum RESET voltage of -1.2 V are examined. (a) Early RESET failures from "Hf" and "Ti" electrodes, (b) stable switching cycles of SET and RESET from "Ta" and "W" electrodes.

Since the Hf- and Ti-based devices show the early RESET failure, only the W- and Ta-OE based Ta_2O_5 ReRAM devices are further investigated and compared under identical bias conditions. Fig. 4(a) shows a typical *I-V* characteristics of Ta_2O_5 device at I_{CC} of 1.0 mA exhibiting the gradual RESET transition for two different RESET stop voltages ($V_{RESET\text{-}STOP}$ = -1.4 V & -2.0 V). The higher RESET voltage toggles the device into a higher R_{HRS} value [15, 28-30], which subsequently results in a higher SET voltage. This phenomenon is attributed to the fact that under the electric field during RESET, the V_O's drift away from the high WF metal electrode resulting in an increase of the effective Schottky barrier height. This drift, however, builds up a concentration gradient giving rise to an opposite diffusion flow of V_O. Hence, the V_O distribution approaches an equilibrium (balance) over time [15]. This equilibrium profile is frozen in when the voltage is switched off and depends on the maximum applied RESET voltage. When the RESET voltage increases, the Ta_2O_5 close to the high WF metal electrode becomes more depleted from V_O's and, thus, the resulting R_{HRS} value becomes higher [15, 31-34]. The effects of the $V_{RESET\text{-}STOP}$ on the R_{HRS} for the W- and the Ta-OE based Ta_2O_5 devices are investigated in the range of -1.4 V to -2.0 V with -0.2 V increment under identical SET I_{CC} of 1.0 mA using quasi-static voltage sweeps. The W-OE devices consistently yield higher R_{HRS} than the Ta-OE devices, shown in Fig. 4(b). For $V_{RESET\text{-}STOP}$ = -1.4 V, the R_{HRS} value of the Ta_2O_5 ReRAM with the W-OE is 23 kΩ in comparison with 2.0 kΩ for

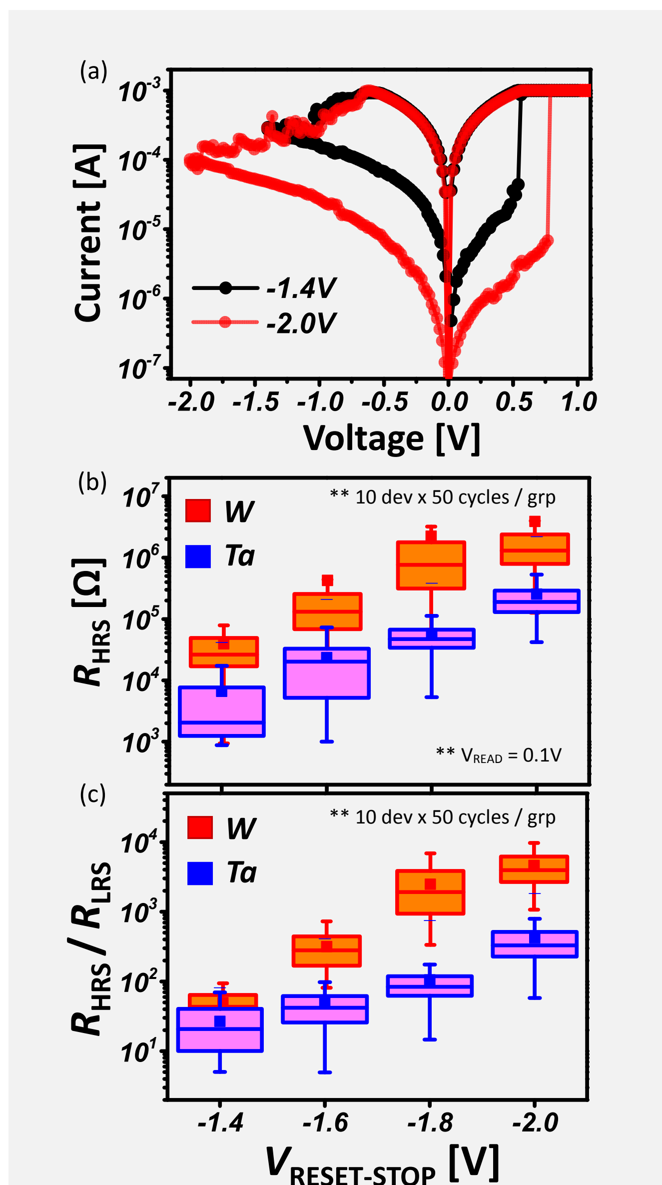

Fig. 4. (a) Typical SET-RESET characteristics of the Ta_2O_5 ReRAM device for two different $V_{RESET\text{-}STOP}$ conditions (-1.4 V, -2.0 V), (b) R_{HRS} change depending on $V_{RESET\text{-}STOP}$ increment for two ohmic electrode materials (W and Ta), (c) Comparison of R_{HRS} / R_{LRS} ratio as a function of the $V_{RESET\text{-}STOP}$ increment for the Ta- and the W-OE ReRAM device.

the Ta-OE devices. At $V_{RESET\text{-}STOP}$ = -2.0 V, the R_{HRS} value is further increased to 1.2 MΩ and 200 kΩ for the W- and the Ta-OE device, respectively. Due to the high R_{HRS} for the W-OE device with similar R_{LRS}, the R_{HRS}/R_{LRS} ratio of the W-OE based Ta_2O_5 device is more than 1,000 at $V_{RESET\text{-}STOP}$ =-1.8 V. This is about 12 times higher than the one for the Ta-OE device as shown in Fig. 4(c). The AC RESET behavior of the Ta- and W-OE based Ta_2O_5 devices is further investigated using voltage pulses of 100 ns and 100 μs length. The measurement schematics of AC pulse sequences are shown in Fig. 5(a). The R_{LRS} of all devices is always kept constant to about 400 Ω, which is verified by a 0.1 V read pulse with 1.0 μs width before the RESET pulse application. Fig. 5 (b) shows the R_{HRS} change for different RESET voltages ranging

This journal is © The Royal Society of Chemistry 20xx

Please do not adjust margins

Please do not adjust margins

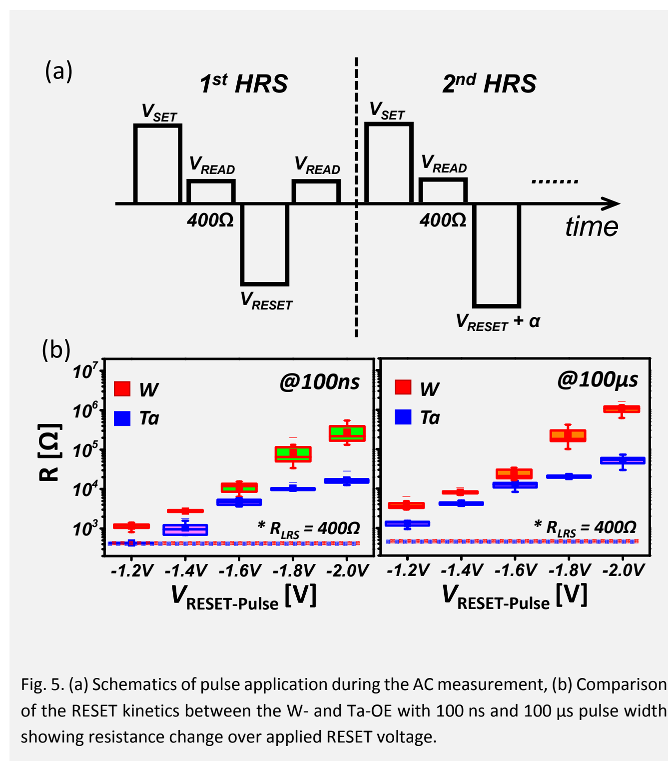

Fig. 5. (a) Schematics of pulse application during the AC measurement, (b) Comparison of the RESET kinetics between the W- and Ta-OE with 100 ns and 100 µs pulse width showing resistance change over applied RESET voltage.

from -1.2 V to -2.0 V at both 100 ns and 100 µs pulse widths. For both, the W- and Ta-OE devices, the R_{HRS} state varies with the pulse voltage amplitude. For both pulse widths, the rate of resistance change over voltage amplitude is steeper for the W-OE than that of the Ta-OE device. For the 100 ns pulse width, at the $V_{RESET\text{-}PULSE}$ = -2.0 V, the R_{HRS} of the W-OE based Ta_2O_5 device was approximately 15 times (221 kΩ for W vs. 16 kΩ for Ta) higher than that of Ta-OE device. For the longer RESET pulse (100 µs) at $V_{RESET\text{-}Pulse}$ = -2.0 V, the resistance of the W-OE device was about 20 times (1.1 MΩ for W vs. 53 kΩ for Ta) higher than that of Ta-OE device. As expected, longer pulses (100 µs) result in a higher resistance change than the short pulses (100 ns) for both device stacks at given voltage amplitude [35]. The RESET pulse experiment is consistent with the DC-RESET results where the W-OE shows higher R_{HRS} at any given RESET voltage. The results from both AC and DC measurements thus confirm that the OE material affects the RESET switching speed and equilibrium in the device, which verifies the presumption that oxygen exchange at the OE/metal-oxide interface actively contributes to the switching process.

Next, the SET kinetics of the Ta_2O_5 device for both OE have been investigated with varying amplitudes $V_{SET\text{-}Pulse}$, as shown in Fig. 6(a). The transient SET pulse (in gray) and its corresponding transient SET current ($I_{SET\text{-}Pulse}$) in blue is measured for $V_{SET\text{-}Pulse}$ = 1.2 V and 1.45 V with Ta-OE device. Prior to the SET pulse application, the R_{HRS} value for both conditions was kept between 150 kΩ to 200 kΩ. In the beginning of the $V_{SET\text{-}Pulse}$, the corresponding $I_{SET\text{-}Pulse}$ is relatively low. However, after some time the current level shows a sudden increase. The point in time at which this abrupt increase in the current is observed, is defined as SET switching time, t_{SET}. For the lower $V_{SET\text{-}Pulse}$ (1.2 V), a longer t_{SET} (45 ns) is required to

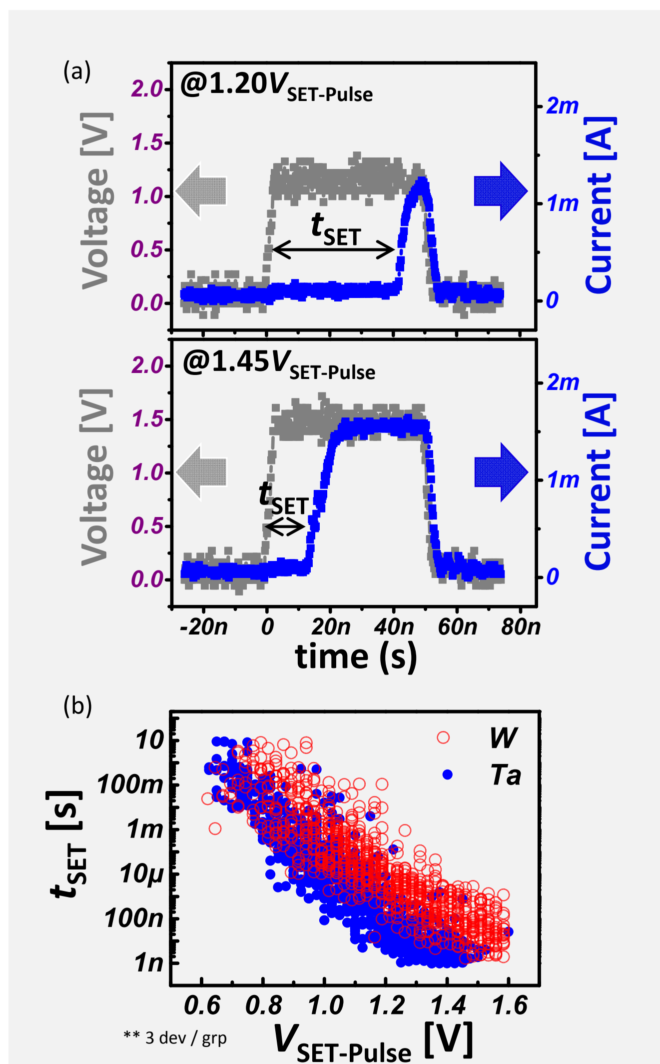

Fig. 6. (a) Examples of the measured transient current (in blue) and the applied SET pulse (in gray) of V_{SET} = 1.3 V and 1.75 V. The abrupt increase of current is identified as the SET process. The SET time (t_{SET}) is obtained depending on the amplitude of SET pulse. (b) A correlation between the t_{SET} and the SET Pulse amplitude for both W- (in red) and Ta-OE (in blue) illustrating the ultra-high nonlinearity of the SET kinetics..

switch the device to the LRS whereas a shorter t_{SET} (15 ns) is observed at the higher $V_{SET\text{-}Pulse}$ (1.45 V). This measurement has been carried out over a wide $V_{SET\text{-}Pulse}$ range spanning from 0.6 V to 1.6 V with 25 mV increment for each OE, shown in Fig. 6(b). A clear correlation between $V_{SET\text{-}Pulse}$ and t_{SET} is observed for both devices. As the $V_{SET\text{-}Pulse}$ increases, the t_{SET} becomes shorter as reported for other devices [36-38]. For the complete voltage range the Ta-OE devices show the shorter t_{SET} i.e. faster SET process. So, the transition from R_{HRS} to R_{LRS} for the SET process appears faster with Ta-OE, which is the exactly opposite to the RESET process of the device (that is faster for the W-OE). This outcome further supports the assumption that the OE plays an active role during the switching process.

Please do not adjust margins

Please do not adjust margins

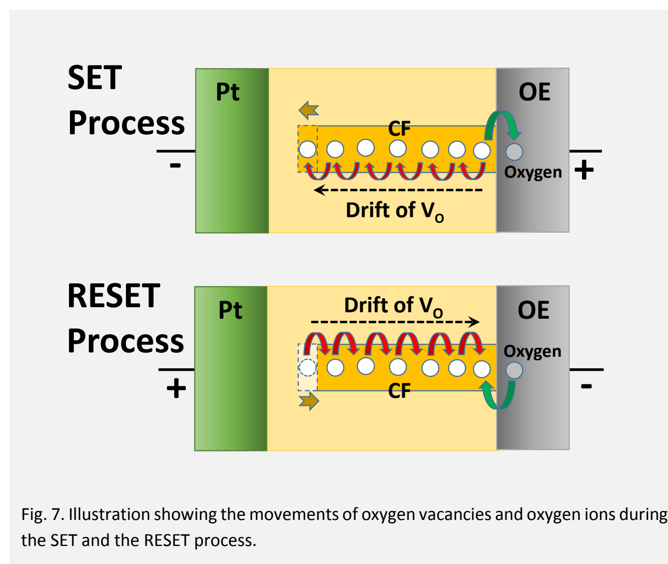

Fig. 7. Illustration showing the movements of oxygen vacancies and oxygen ions during the SET and the RESET process.

Discussion

The experimental results indicate that the OE plays an active role during the switching process in VCM ReRAM devices. In analogy to the forming process, an oxygen exchange reaction occurs during switching at the OE/metal-oxide interfaces. Thus, the former assumptions of the switching process, in which the amount of V_O in the filament stays constant needs to be modified [39]. In addition to the movement of the V_O's in the filament, an oxygen exchange takes place at the OE/oxide interface. Hence, the total amount of the V_O's within the filament changes during the switching process. This modified switching model is illustrated in Fig. 7. During the SET transition, the oxygen vacancies drift towards the high WF metal electrode and decrease the Schottky barrier height. This is corresponding to oxygen moving towards the OE interface, where due to the oxygen exchange reaction oxygen is extracted from the metal-oxide and incorporated in the OE. By this, the electrode may be locally oxidized forming a sub-oxide (which would be still be very conductive), while the total amount of the V_O in the metal-oxide increases (cf. equation 3, proceeding to the left). During the RESET process, the opposite movement of the V_O's result in their depletion at the high WF metal electrode and accumulation at the OE electrode. Due to the oxygen exchange reaction at the electrode, oxygen is incorporated in the oxide layer lowering the amount of vacancies at the OE interface. Thus, the total amount of the V_O's decreases in the oxide layer. The rate of this oxygen exchange reaction depends on E_{VO}. A faster extraction of the oxygen ion from the switching oxide layer (SET) is achieved for a lower (positive) E_{VO} values. In contrast, the re-incorporation of oxygen ions into the switching oxide layer (RESET) is faster for higher (positive) E_{VO}. Thus, a higher E_{VO} is beneficial for faster RESET operation.

The experimental observations can now be explained in the context of the modified model. The early RESET failure occurs in the Ti- and Hf-OE devices. For those two electrodes, E_{VO} is

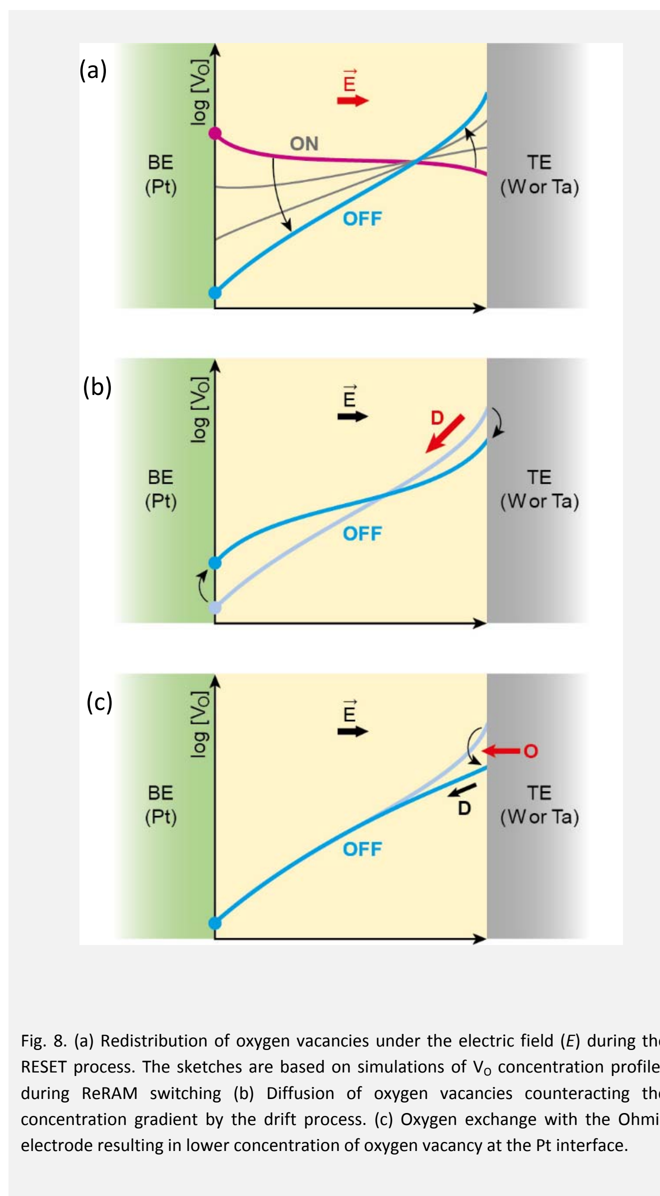

Fig. 8. (a) Redistribution of oxygen vacancies under the electric field (*E*) during the RESET process. The sketches are based on simulations of V_O concentration profiles during ReRAM switching (b) Diffusion of oxygen vacancies counteracting the concentration gradient by the drift process. (c) Oxygen exchange with the Ohmic electrode resulting in lower concentration of oxygen vacancy at the Pt interface.

negative, i.e. there is a continuous thermodynamic drive for V_O formation. Kinetic barriers to this may be lowered due to Joule heating during the switching process, with oxygen extraction from Ta_2O_5 strongly enhanced during the SET process while O re-incorporation during RESET process is strongly reduced. Hence, the total amount of the oxygen vacancies is increasing from cycle to cycle, reducing the film resistivity. Eventually, the current and the dissipated power during the RESET process is so high that oxygen may get excorporated at the opposite Pt electrode (i.e., we get a spurious SET at this Pt electrode), resulting in an overall RESET failure. For the Ta- and W-OE devices, the oxygen exchange during the SET and the RESET process is better balanced and thus stable switching is obtained. The different speed of the RESET process for these devices can also be explained with the oxygen exchange model. Fig. 8 sketches the change in the oxygen vacancy profiles during the RESET process, where the profiles are motivated by previous simulation results [14, 15]. During the RESET process, the

 This journal is © The Royal Society of Chemistry 20xx

Please do not adjust margins

Please do not adjust margins

oxygen vacancies are depleted near the high WF Pt electrode and pile up at the OE interface by redistribution of charged oxygen vacancies (Vö) under the electric field (*E*), as shown in Fig. 8(a). The depletion at the high WF Pt electrode results in a space charge region and a high barrier height blocking the electron conduction. The diffusion (D) of the V_O will counteract the concentration gradient build-up by the drift, resulting in equilibrium in Fig. 8(b). By that, the V_O accumulation at the OE will be reduced. However, these amount of the V_O will diffuse towards the high WF Pt electrode, decreasing the depletion and increasing the current in the R_{HRS}. The oxygen (O) exchange with the OE will reduce the high V_O concentration lowering the back-diffusion force (D), shown in Fig. 8(c). As the result, a lowered concentration of the V_O at the high WF Pt interface can be maintained and the leakage current remains low. The W-OE can release oxygen (O) back easier than the Ta-OE due to its higher energy for defect formation. This is why the W-OE can achieve lower leakage current (higher R_{HRS}) with the same V_{RESET} application. In contrast, for the switching speed of the SET process, the Ta-OE is faster than the W-OE. This is attributed to the speed of the oxygen exchange reaction at the interface. The extraction of the oxygen ions at the OE electrode is faster for the Ta-OE because it has the lower E_{VO}.

Conclusions

In this study, Ta_2O_5-based ReRAM devices have been studied with W, Ta, Ti and Hf-OEs. Based on our experimental observations, a modified switching model is proposed. In contrast to the previous models, the experimental results show that oxygen exchange reactions with the ohmic electrode not only occur during deposition and the electroforming process, but also during each SET and RESET process. The relevant design property presumably is the interfacial oxygen defect formation energy E_{VO} at the OE/oxide interface. The Ti- and Hf-OE devices suffer from an early RESET failure due to an accumulation of the V_O's during the switching cycles. This is explained by their negative E_{VO}, which favors the reduction of the switching oxide layer. In contrast, the positive E_{VO} for the Ta- and W-OE leads to highly stable switching process in the Ta_2O_5 ReRAM. The W-OE devices show an increased R_{HRS} compared with the Ta-electrode under identical RESET conditions. This difference of the R_{HRS} value can also be explained by the oxygen exchange reaction. The E_{VO} of W/Ta_2O_5 favors incorporation of the oxygen ions into the switching oxide layer decreasing the total amount of the V_O inside the switching oxide, which will lower the current in high resistance state under the given biasing conditions of the RESET process. On the opposite side, the lower E_{VO} for Ta-OE results in faster SET processes than its counterpart W-OE. These observations indicate that oxygen interchange with the OE plays an important role during the resistive switching, leading to extended modified switching model. The proposed model can explain the experimental dependence of the resistive switching properties as RESET depth and SET speed on the used material stack, and so will be beneficial for the future material´s design of optimized ReRAM devices.

Acknowledgements

This work was supported by the German Research Foundation (DFG) within the framework of SFB 917, Nanoswitches and the authors thank Dr. Daesung Park and Mr. Sebastian Zischke from Central Facility for Electron Microscopy (GFE), RWTH Aachen for the cross-sectional TEM images, and Dr.Ilia Valov from Peter Grünberg Institute, Forschungszentrum Jülich for critical review of the manuscript.

References

1. M.-J. Lee, C. B. Lee, D. Lee, S. R. Lee, M. Chang, J. H. Hur, Y.-B. Kim, C. -J. Kim, D. H. Seo, S. Seo, U.-I. Chung, I.-K. Yoo, and K. Kim, *Nature Materials*, 2011, **10**, 625.
2. M. Fujimoto, H. Koyama, M. Konagai, Y. Hosoi, K. Ishihara, S. Ohnishi, and N. Awaya, *Applied Physics Letters,* 2006, **89**, 223509/1.
3. R. Waser and M. Aono, *Nature Materials*, 2007, **6**, 833.
4. A. Wedig, M. Luebben, D.-Y. Cho, M. Moors, K. Skaja, V. Rana, T. Hasegawa, K. Adepalli, B. Yildiz, R. Waser, and I. Valov, *Nature Nanotechnology*, 2016, **11**, 67.
5. F. A. Kroeger and H. J. Vink, *Solid State Physics*, 1956, **3**, 307.
6. D. Ielmini and R. Waser, *Wiley-VCH*, 2016
7. S. Stille, C. Lenser, R. Dittmann, A. Koehl, I. Krug, R. Muenstermann, J. Perlich, C. M. Schneider, U. Klemradt, and R. Waser, *Applied Physics Letters*, 2012, **100**, 223503/1.
8. A. Sharma, M. Noman, M. Abdelmoula, M. Skowronski, and J. Bain, *Advanced Functional Materials*, 2014, **24**, 5522.
9. R. Waser and M. Wuttig, *2009 Proceedings of Esscirc*, 2009, 66.
10. J. J. Yang, F. Miao, M. D. Pickett, D. A. A. Ohlberg, D.R. Stewart, C. N. Lau, and R. S. Williams, *Nanotechnology*, 2009, **20**, 215201.
11. R. Waser, R. Dittmann, G. Staikov, and K. Szot, *Advanced Materials*, 2009, **21**, 2632.
12. J. J. Yang, M. D. Pickett, X. Li, D. A. A. Ohlberg, D. R. Stewart, and R. S. Williams, *Nature Nanotechnology*, 2008, **3**, 429.
13. J. H. Hur, M.-J. Lee, C. B. Lee, Y.-B. Kim, and C.-J. Kim, *Phys. Rev. B*, 2010, **82**, 155321.

This journal is © The Royal Society of Chemistry 20xx

Please do not adjust margins

Please do not adjust margins

14. A. Marchewka, R. Waser, and S. Menzel, *2015 International Conference On Simulation of Semiconductor Processes and Devices (SISPAD), 9-11 September, Washington D.C, USA*, 2015, 297.

15. A. Marchewka, B. Roesgen, K. Skaja, H. Du, C.-L. Jia, J. Mayer, V. Rana, R. Waser, and S. Menzel, *Advanced Electronic Materials*, 2016, **2**

16. A. C. Torrezan, J. P. Strachan, G. Medeiros-Ribeiro, and R. S. Williams, *Nanotechnology*, 2011, **22**, 485203.

17. C. Chen, L. Goux, A. Fantini, A. Redolfi, S. Clima, R. Degraeve, Y. Chen, G. Groeseneken, and M. Jurczak, *Technical Digest - International Electron Devices Meeting, IEDM*, 2015, **2015-February**, 14.2.1.

18. L. Goux, A. Fantini, Y. Y. Chen, A. Redolfi, R. Degraeve, and M. Jurczak, *Ecs Solid State Letters*, 2014, **3**, Q79.

19. C. Hsu, C. Wan, I. Wang, M. Chen, C. Lo, Y. Lee, W. Jang, C. Lin, and T. Hou, *Electron Devices Meeting (IEDM), 2013 IEEE International*, 2013, 10.4.1.

20. A. Prakash, D. Jana, and S. Maikap, *Nanoscale Research Letters*, 2013, **8**, 1.

21. W. Kim, B. Rösgen, T. Breuer, S. Menzel, D. Wouters, R. Waser, and V. Rana, *Microelectronic Engineering*, 2016, **154**, 38.

22. J. J. Yang, J. P. Strachan, F. Miao, M. Zhang, M. D. Pickett, W. Yi, D. A. A. Ohlberg, G. Medeiros-Ribeiro, and R. S. Williams, *Applied Physics A: Materials Science & Processing*, 2011, **102**, 785.

23. Y. S. Chen, H. Y. Lee, P. S. Chen, P. Y. Gu, W. H. Liu, W. S. Chen, Y. Y. Hsu, C. H. Tsai, F. Chen, M. J. Tsai, and C. Lien, *IEEE Electron Device Letters*, 2011, **32**, 390.

24. Y. Guo and J. Robertson, *Applied Physics Letters*, 2014, **105**, 222110.

25. Y. Guo and J. Robertson, *Applied Physics Letters*, 2014, **105**, 223516/1.

26. J. Robertson and S.J. Clark, *Physical Review B: Condensed Matter*, 2011, **83**, 075205 1.

27. Y. Guo and J. Robertson, *Applied Physics Letters*, 2014, **105**, 223516.

28. L. Goux, Y. Chen, L. Pantisano, X. Wang, G. Groeseneken, M. Jurczak, and D. J. Wouters, *Electrochemical and Solid State Letters*, 2010, **13**, G54.

29. F. Nardi, S. Larentis, S. Balatti, D. Gilmer, and D. Ielmini, *IEEE Transactions on Electron Devices*, 2012, **59**, 2461.

30. S. Yu, Y. Wu, R. Jeyasingh, D. Kuzum, and H. P. Wong, *IEEE Transactions on Electron Devices*, 2011, **58**, 2729.

31. S. Larentis, C. Cagli, F. Nardi, and D. Ielmini, *Microelectronic Engineering*, 2011, **88**, 1119.

32. D. Ielmini, *IEEE Transactions on Electron Devices*, 2011, **58**, 4309.

33. K. Kim, D. S. Jeong, and C. S. Hwang, *Nanotechnology*, 2011, **22**

34. J. Y. Son and Y.-H. Shin, *Applied Physics Letters*, 2008, **92**, 222106.

35. H. Schroeder, V. V. Zhirnov, R. K. Cavin, and R. Waser, *Journal of Applied Physics*, 2010, **107**, 054517/1.

36. S. Menzel, M. Salinga, U. Böttger, and M. Wimmer, *Adv. Funct. Mater.*, 2015, **25**, 6306.

37. Y. Nishi, K. Fleck, U. Boettger, R. Waser, and S. Menzel, *IEEE Transactions on Electron Devices*, 2015, **62**, 1561.

38. Y. Nishi, S. Menzel, K. Fleck, U. Boettger, and R. Waser, *IEEE Electron Device Letters*, 2013, **PP**, 1.

39. R. Degraeve, A. Fantini, S. Clima, B. Govoreanu, L. Goux, Y.Y. Chen, D.J. Wouters, Ph. Roussel, G.S. Kar, G. Pourtois, S. Cosemans, J.A. Kittl, G. Groeseneken, M. Jurczak, and L. Altimime, *Proceedings of the 2012 Symposium on VLSI Technology*, 2012, 75.

This journal is © The Royal Society of Chemistry 20xx

Please do not adjust margins